Highlights

Real-world implementation and evaluation of a Model Predictive Control framework in an office space

Maximilian Mork, Florian Redder, André Xhonneux, Dirk Müller

- Experimental implementation of Modelica-based MPC in an office building
- Operation of dynamic and inert heating actuators
- Operation of Venetian blinds for solar shading
- Implementation of parameter estimation, state estimation and disturbance forecasting
- MPC results exhibit energy-efficient heating and shading control with low discomfort

Real-world implementation and evaluation of a Model Predictive Control framework in an office space

Maximilian Mork[a,*], Florian Redder[a], André Xhonneux[a], Dirk Müller[a,b]

[a] *Institute of Energy and Climate Research - Energy Systems Engineering (IEK-10), Forschungszentrum Jülich GmbH, Wilhelm-Johnen-Straße, Jülich, 52428, Germany*
[b] *Institute for Energy Efficient Buildings and Indoor Climate, E.ON Energy Research Center, RWTH Aachen University, Mathieustraße 10, Aachen, 52074, Germany*

Abstract

In this work, Model Predictive Control (MPC) is experimentally implemented on a Heating, Ventilation and Air Conditioning (HVAC) system of a large-scale office space. As controller model, a physics-based Modelica building model is calibrated based on historic data pursuing an iterative, nonlinear optimization approach. For the calibration period with a horizon of seven weeks, the calibrated model exhibits a high model accuracy with a Root Mean Square Error (RMSE) of 0.49 K between the measured and estimated room temperature. The MPC toolchain includes modules for state estimation and forecasts of disturbances quantities (such as outdoor temperature, solar radiation including calculation of the direct and diffuse fraction, supply temperatures and occupancy). The MPC execution comprises the operation of heating based on radiators and floor heating (via regulation of valve openings) as well as shading of three Venetian blind systems (via regulation of vertical position and slat inclination angle). The experiment is conducted during a heating period with a duration of three weeks from October 21 to November 11, 2022. The heating actuators are controlled considering their typical dynamics and take into account the night setback during unoccupied office periods. User acceptance of the automated shading control is included through an additional cost function terms for the shading operation. The field test reveals the predictive control capabilities of the proposed MPC toolchain in a real-life scenario, demonstrating energy-efficient building operation and total average discomfort of 0.53 Kh/d. The MPC formulation provides flexibility regarding tunability of the control towards energy efficiency, thermal comfort, daylight transmission and non-oscillating shading control. Finally, the disturbance forecast accuracies for outdoor temperature and the solar radiation quantities are evaluated and the MPC control performance is compared against a conventional control approach.

Keywords:
Model Predictive Control (MPC), Building control, Building energy system, Experimental MPC, HVAC, Modelica

Nomenclature

Abbreviations

AHU	Air Handling unit
dhi	diffuse horizontal irradiance

*Corresponding author
Email address: m.mork@fz-juelich.de (Maximilian Mork)

DWD	Deutscher Wetterdienst
ETS	Engineering-Tool-Software
FMI	Functional Mockup Interface
ghi	global horizontal irradiance
HVAC	Heating, Ventilation and Air Conditioning
illum	illuminance
MAE	Mean Average Error
MOSMIX	Model Output Statistics-MIX
MPC	Model Predictive Control
MQTT	Message Queuing Telemetry Transport
PID	Proportional-Integrative-Differential
RBC	Rule-Based Control
RMSE	Root Mean Square Error
TABS	Thermally Activated Building Systems
UKF	Unscented Kalman Filter

Subscripts

al	artificial lighting
dl	daylight
floorHeat	floor heating
inclAng	inclination angle
Light	lighting
max	maximum
min	minimum
posShad	shading position
rad	radiator
set	set-point

1. Introduction

Approximately 30 % of the global energy demand and 27 % of the global CO_2 emissions are attributed to the building sector (excluding the building construction industry) [1]. Heating, Ventilation and Air Conditioning (HVAC) systems provide comfort to building users and contribute to a major extent to the energy consumption in buildings [2]. Thus, energy-efficient control of these systems offers a large potential for the increase in building energy efficiency and reduction of global energy demand. Compared to other measurements to increase the energy efficiency of buildings such as improvements of the building envelope, refurbishments or replacements, the optimization of the control of HVAC systems is a cost-effective and practicable approach.

The control of HVAC systems poses various challenges due to nonlinear dynamics with time delays, conflicting optimization goals (e.g., the simultaneous minimization of energy consumption and discomfort) as well as system dynamics, setpoints and disturbances that vary with time [3]. As people in industrialized countries spend on average 90 % of their time in buildings, there are high demands on comfort (e.g., thermal, indoor air quality and visual), which has an impact on occupant productivity, satisfaction and health [4].

Conventional control strategies for buildings are Rule-Based Control (RBC) or Proportional-Integrative-Differential (PID) controllers as they represent easy-to-implement controllers with low computational requirements [5]. They need to be tuned for specific operating ranges, perform badly outside the tuning conditions, are not able to integrate system and comfort constraints or future disturbances, to operate time-varying system dynamics or time delay and to deal with conflicting optimization goals.

Model Predictive Control (MPC) is an advanced control technique, which has attracted attention in the building control domain and suggests various benefits compared with conventional controllers addressing the aforementioned challenges. MPC builds upon a model of the building energy systems to predict future system behavior and calculate control inputs in an anticipatory manner. It is able to integrate system and comfort constraints as well as forecasted disturbances, control buildings with time-varying dynamics and time delay as well as minimize multi-objective cost functions over a prediction horizon. Beneficial buildings characteristics for the application of MPC are high thermal mass, thermal storage, wide comfort ranges, predictable heat gains and inert HVAC systems with time delay [6, 7].

1.1. Background

MPC has demonstrated its functionality and benefits of energy savings and simultaneous preservation or even improvement of thermal comfort in a wide range of simulative case studies and beyond that, in some field demonstrations. Cigler et al. [8] applied MPC to the control of a ceiling radiant heating and cooling system in an office building in Prague achieving energy savings of 15 to 28 % compared to the conventional heating curve based control. Applying MPC to the operation of a large cooling system in a university building in Merced, California, Ma et al. [9] obtain an increase of 19 % in efficiency in terms of a coefficient of performance compared to a reference control. The practical implementation of building MPC demonstrated energy savings of more than 20 % controlling a ventilation system in a research laboratory in Illinois [10], 17 % in an office building in Belgium operating Thermally Activated Building Systems (TABS) [11], 19 % in two office buildings in Australia controlling Air Handling Units (AHUs) [12] and more than 20 % of primary energy reduction for an office building in Brussels operating heat pumps and gas boiler [13]. These figures coincide with thermal energy savings of 16 % in comparison with an identically configured cell controlling a radiant slab system in a building test facility in Berkeley, California, [14], energy savings of 15 to 20 % in a laboratory in Bari, Italy, controlling fan coil units [15] and electrical energy savings of 15 to 21 % in a test facility in Singapore with two identical experimental cells controlling mechanical ventilation, shading and lighting [16]. Higher energy savings were obtained by Drgoňa et al. [17] with more than 50 % employing MPC for the operation of a heat pump, floor heating and TABS in an office building in Belgium, by Freund and Schmitz [18] with energy savings of 30 % implementing MPC for TABS supply temperature control in a large-scale office building in Hamburg, Germany, by Blum et al. [19] with energy savings of 40 % executing MPC on an HVAC system of an office building in Berkeley, California, and by Merema et al. [20] with up to 55 % of heating energy savings applying MPC to a ventilation system of an educational building in Ghent, Belgium.

When implementing MPC in building energy systems, the modeling part plays a crucial role for the success of MPC, as it consumes most of the project time and costs [8, 21]. This is attributable to the unique characteristics of every building requiring an individual, tailored modeling for every MPC implementation. Thus, a user-friendly, accurate and fast generation of suitable MPC models is essential for the widespread applicability of MPC in building control, also on a commercial scale.

The modeling language Modelica [22] fulfills these requirements and suits the tailored building modeling due to its flexible and modular structure. It is an open-source, equation-based and object-oriented modeling language, which allows the collection of modular, reusable models in libraries. The generation of open-source building simulation libraries in Modelica is advanced by international projects such as the IEA EBC Annex 60 project, which resulted in the Modelica IBPSA library [23]. This base library has been extended by several research groups into individual libraries, which are still actively developed and maintained and contain an extensive range of models for buildings and HVAC systems [24, 25, 26, 27]. Reusing component models of these shared, open-source libraries enables modular, high-accuracy modeling and avoids repetitive modeling efforts. The user-friendliness of Modelica is further increased, as it is equipped with a graphical user interface to connect components. Modelica supports the Functional Mockup Interface (FMI) standard, which allows for model exchange and co-simulation with other modeling and simulation tools. The language extension Optimica [28] enables the formulation of optimization problems by adding constraints, variable bounds and objective functions to the simulation model.

To suit the use in a building MPC, on the one hand, a model has to be simple and computationally efficient enough to be solved in an adequate amount of time, on the other hand, it has to be detailed enough

to reproduce the dynamics of the building in an accurate manner. Particularly for use in MPC, a model of high accuracy is crucial as an MPC tends to operate the comfort quantities (e.g., temperature or CO_2 concentration) near their specified bounds to save energy, where an inaccurate model would risk comfort violations due to errors in predicting the building dynamics.

Nonlinearities appear in buildings within specific physical heat transfer phenomena in the building envelope (e.g., convection, radiation or absorption/transmission of solar gains through windows), in HVAC systems (e.g., heat pumps, fans, pumps, valves and in general, hydraulic relationships between pressure difference and mass flow rate) and corresponding performance curves and tables. Especially for the nonlinear dynamics in HVAC systems, nonlinear physics-based controller models are more accurate over a wide range of operating conditions compared with models that are linearized around a nominal operating point. Nonlinear MPC enables higher flexibility in formulating the optimization problem consisting of system dynamics, constraints and cost function and unlocks an exploitable MPC potential (i.e., in the form of energy or cost savings) closer to the theoretical performance bound [29]. In linear MPC, which is the most commonly applied building MPC form [30], usually, only intermediate quantities (e.g., heating or cooling energy flows) or high-level set-points are calculated by the optimization minimizing an approximation of the nonlinear cost function, whereas the conversion into the building actuator control signals is assigned to a post-processing or suboptimal low-level controller (e.g., PID or RBC). By applying nonlinear MPC, the optimization is executed with respect to the control inputs that are actually implemented in actuators and efforts for pre- and post-processing, variable mapping and linearization are reduced. The increased model accuracy comes at the expense of higher optimization complexity and computational demand; however, optimization algorithms and solvers are continuously improving and due to advancements of processors and cloud computing the available computational power, is increasing exponentially [5].

1.2. Contribution

In this work, a practical toolchain for nonlinear, Modelica-based MPC is demonstrated in a field test on an HVAC system of an office space. The work contributes to bridging the gap between the high number of simulative MPC implementations and the scarce cases of practical realizations of building MPC. The model generation pursues a physics-based modeling approach mapping each physical component to a model equivalent based on a building simulation library and documentation of the building envelope and HVAC systems. The modeling approach preserves interpretability of the physically meaningful model parameters/states and optimization results alleviating spatial location, comprehension of system behavior and fault detection. For refining the model, an iterative, nonlinear parameter estimation calibrates selected parameters of the Modelica model. The MPC toolchain contains modules for forecasting disturbance quantities (occupancy and weather including solar radiation quantities) and state estimation. In the field test, both heating (via manipulation of the valve openings of floor heating and radiators) and shading (via manipulation of the angle and position of Venetian blinds) are operated over a period of 21 days.

The paper is structured as followed as follows: In Section 2 the test bed for applying the MPC toolchain is described. Section 3 presents the implemented toolchain, including modules for forecasting, state and parameter estimation as well as communication with sensors, actuators and databases. In Section 4 the MPC formulation for the experimental case study is specified. Section 5 presents the results of the parameter estimation, MPC execution, evaluation of the disturbance forecast accuracy and a reference application of a conventional control approach. Finally, Section 6 summarizes the results and gives an outlook on improvements and ongoing development of the toolchain.

2. Case study building

The developed MPC toolchain is demonstrated under real-life conditions and applied to a room of the student laboratory *JuLab* on the campus of the Forschungszentrum Jülich. The controlled room is also known as "Gläsernes Labor" ("glass laboratory", front room on the ground floor in Figure 1). It has three extensive window facades, a floor area of approximately 120 m^2 and is dedicated to laboratory exercises for visiting pupils. The room is equipped with facade-individual Venetian blinds, two radiators and floor heating

and thus, integrates both a heating system with fast and slow dynamics. The radiators and floor heating are equipped with electromechanical control valves, which allow for setting the valve openings directly. The three window facades are oriented in the south-east (SE), south-west (SW) and north-west (NW) direction. A sketch of the room structure and its orientation is given in Figure 2. The room has six small windows in the form of manually openable skylights (visible in Figure 1 above the doors and in Figure 2 on the window facades). To accurately monitor occupancy, a person counter is installed, which detects the current number of occupants in the room. Further measuring equipment in the form of a proprietary system monitors building-wide heating energy consumption, heating water volume flows and supply and return water temperatures. Heating consumption measurements are available for the radiator heating circuit and the floor heating circuit separately.

Several sensors are installed in the room, e.g., for temperature, CO_2, illuminance as well as window and door opening states. The room temperature sensor is mounted at the internal wall of the room (see localization in Figure 2) and measures at intervals of 0.1 °C. Most of the actuators and sensors employ the building automation standard KNX. Several devices (e.g., the sensors for door and window opening states and the radiators) use the wireless EnOcean technology, but they are fully integrated with the KNX bus via an EnOcean-KNX gateway and addressed via the KNX system. A further KNX-IP gateway ensures the communication the cloud.

Figure 1: JuLab building at Forschungszentrum Jülich

3. Methodology

Figure 3 gives an overview of the toolchain that forms the basis for the practical implementation of the MPC. The dashed box comprises the modules that are executed *online* during the real-time execution of the MPC, namely, the forecasting of the disturbance quantities weather and occupancy, the state estimation and the real-time communication of the actuator control inputs (i.e., MPC outputs) and measurements via the

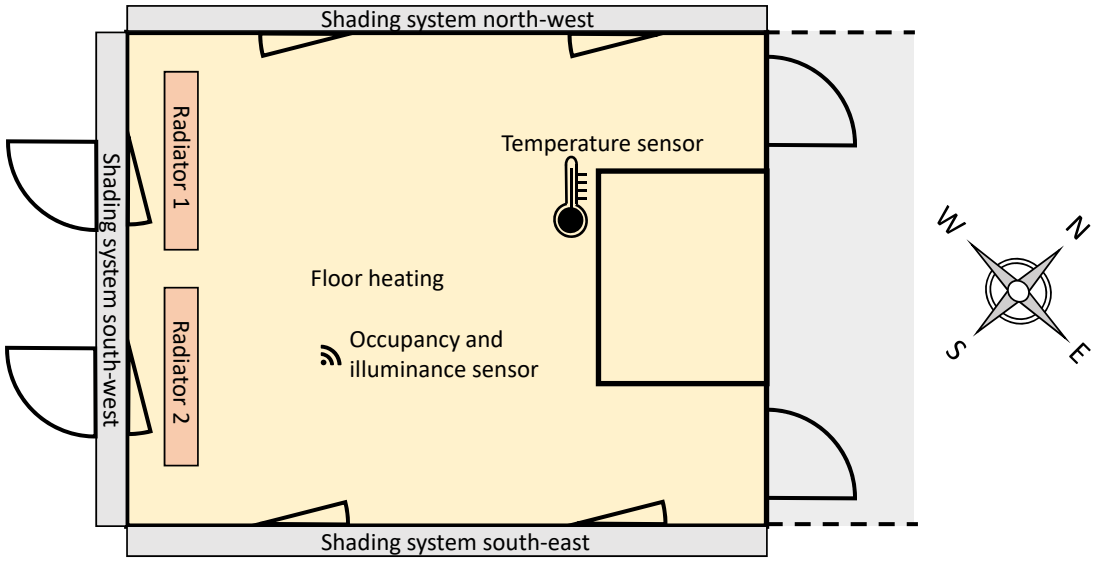

Figure 2: Setup of controlled room

network protocol Message Queuing Telemetry Transport (MQTT). The components outside the box serve the purpose of *offline* calibrating/updating selected parameters of the building model within a parameter estimation based on measurement data retrieved from a database. To this end, historic measurements of both control inputs and sensor values are stored in a database. The implemented toolchain builds upon JModelica.org [28] (using linear HSL solver ma27 [31]), which is a software framework for gradient-based optimization of Modelica models and is equipped with an interface to IPOPT 3.13.1 [32] for nonlinear optimization. In previous works, the MPC framework has been extended by a distributed MPC approach [33] for control of large-scale buildings, a hierarchical MPC [34] for splitting the control complexity in the temporal dimension and a hybrid MPC [35] for the integration of integer decision variables while taking into account nonlinearities. With regard to the interfaced database, access to the Outlook room booking and the MQTT communication with sensors and actuators, this chapter builds upon the work by Redder et al. [36] and Althaus et al. [37]. For a more detailed technical description of these implementations, the reader is referred to these publications. In the following, the different modules of the toolchain are described.

Forecasting

In the forecasting module, the different disturbance quantities that have an impact on the room behavior are forecasted. For the weather quantities, weather forecast data provided by the *Deutscher Wetterdienst* (DWD) are used. The retrieved weather forecast is a statistically optimized *Model Output Statistics-MIX* (MOSMIX) forecast for the location of Jülich and is updated every hour. The forecasted weather quantities comprise ambient temperature, surface pressure, dew point temperature, wind direction and speed, different forms of cloud cover and global horizontal irradiance.

Based on the Python package *pvlib* [38] and several additional solar models presented by Dervishi and Mahdavi [39], the forecasted global horizontal irradiance is split into a diffuse and direct fraction. For this purpose, the *pvlib* provides several models such as the DISC [40] and Erbs model [41]. These models estimate either the direct or the diffuse fraction of the global horizontal irradiance based on empirical relationships using the clearness index (ratio of the global to the extraterrestrial horizontal irradiance) and additional weather quantities such as solar altitude, air temperature and relative humidity. From the models presented by Dervishi and Mahdavi [39], the models proposed by Reindl et al. [42] and Orgill and Hollands [43]

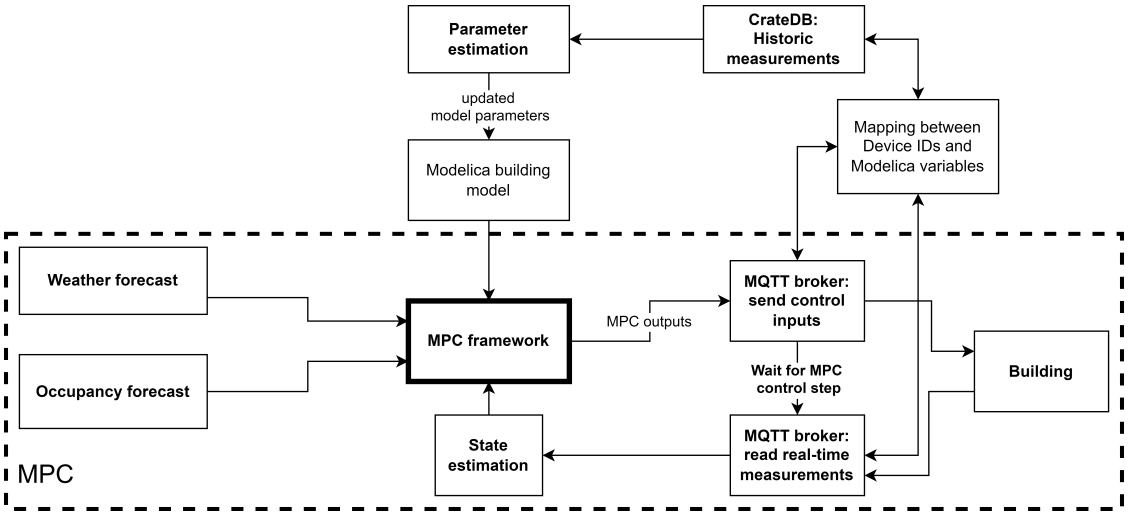

Figure 3: Overview of the toolchain for the practical MPC implementation

are implemented. For the nearest weather station within the Python package *wetterdienst* that provides measured global and diffuse horizontal irradiance (Aachen-Orsbach, approximately 25 km distance from Jülich), the capabilities of the implemented solar models to predict the diffuse horizontal irradiance are evaluated by comparing the predicted with the measured values (evaluation period from September 1 to November 1, 2022). Based on the evaluation results, the DIRINT modification of the DISC model [44] (based on additional dew point temperature information; version provided by the *pvlib*) with the lowest Root Mean Square Error (RMSE) of 27.4 W/m^2 (shown in Figure 4) is chosen for predicting the direct/diffuse solar fractions of the forecasted global horizontal irradiance. The calculated direct and diffuse solar fractions are then used to forecast the direct normal and diffuse horizontal irradiance. For the shading operation and the MPC control performance, the accuracy of the irradiance forecasts is of high relevance due to its large window facades.

Based on the ambient temperature forecast provided by the DWD, the heating water supply temperatures for the floor heating and radiators are forecasted, which are controlled by the building automation system based on heating curves depending on the ambient temperature. Based on historic data from the CrateDB database, a relation between the ambient temperature and the corresponding supply temperature of the floor heating or radiators is calculated in the form of a linear regression model, which is then used in the forecasting module for the prediction of future supply temperatures.

The future number of occupants in the room is forecasted based on a historic look-up table. Access to the Outlook room booking system provides information about past and future meetings including start, end time and meeting subject. Coupled with historic measurements of the person counter, a look-up table is created, which assigns meeting subjects to the average counted number of occupants. Based on the created look-up table, future meeting subjects are mapped to their average historic occupancy. Since the room is equipped with a person counter and the current number of occupants may deviate from its historic average, a correction is applied, which adjusts the occupancy forecast for the next sampling period based on the current measurement. During the MPC execution, all forecasts (weather and occupancy) are updated at intervals of a prespecified number of eight MPC iterations (equivalent to 2 h).

Historic measurements

Historic data of the control inputs and sensor measurements are stored in a CrateDB database. For all control inputs, the set-point that is determined by the MPC and communicated to the actuators is logged. For some control inputs (e.g., the valve openings of the radiator and floor heating as well as the shading

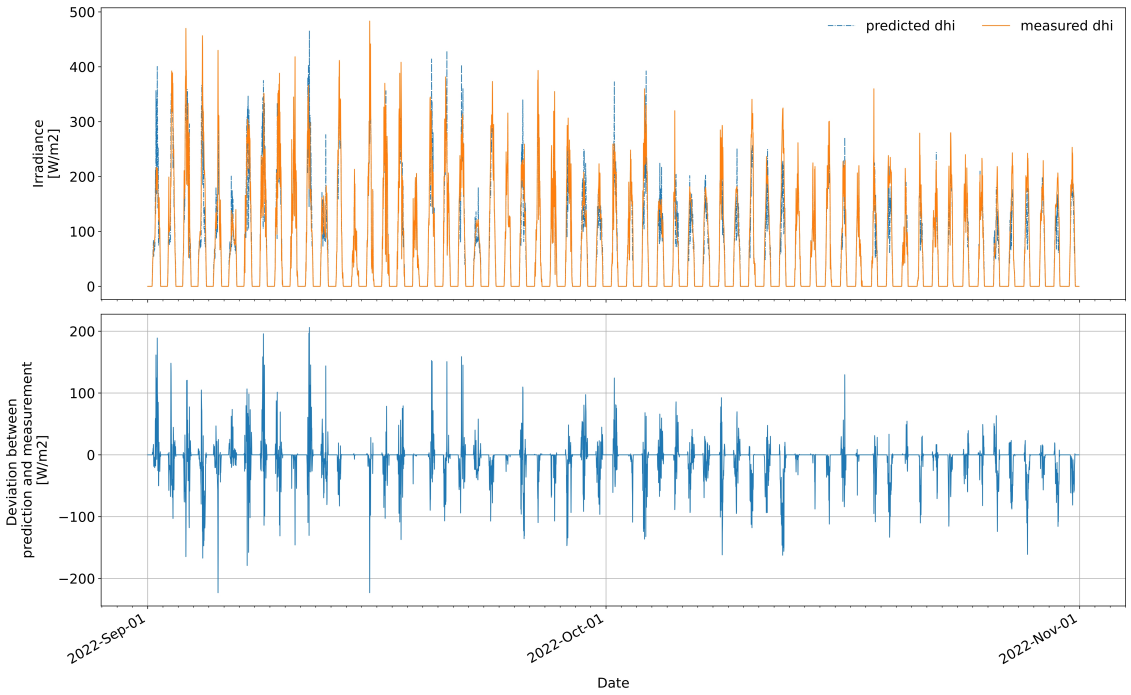

Figure 4: DIRINT modification of the DISC model for the calculation of the direct fraction of the global horizontal irradiance (ghi): RMSE between predicted and measured diffuse horizontal irradiance (dhi): 27.4 W/m^2

control inputs), the feedback of the realized value is stored as well, which enables verification that the sent control inputs are implemented correctly and provides information about the time delay. For accessing the CrateDB, the Python package *crateDB* is used. Based on information from the *Engineering-Tool-Software* (ETS) of the building, which is the software for configuration and parameterization of the KNX building system, KNX group addresses and corresponding descriptions (e.g., sending a set-point for the shading position or getting the current illuminance measurement) are mapped to device IDs. Based on the device IDs and the respective descriptions, a mapping is created between the Modelica model variables and the corresponding device IDs. Since the data are stored at irregular time intervals and mainly in an event-based manner, for use of the data in a parameter estimation, a resampling method is necessary, which resamples the data, e.g., at 15-minute intervals. The resampling is implemented according to the corresponding data type of the device ID, e.g., being a float or integer. Both for the control inputs and integer type data, a forward-fill approach is conducted to resample the time-series data. For the remaining data types, the time-series data are interpolated during resampling.

For the parameter estimation, weather measurements for the site of Jülich are required. The roof-mounted weather station of the building just provides measurements for ambient temperature, wind speed and external illuminance. The latter is measured by illuminance sensors that are oriented in the directions of the window facades (south-east, south-west and north-east). Based on the different illuminance sensor measurements and local global horizontal irradiance measurements, which are available for the period exhibited in Figure 5, a linear regression model is built. It calculates the global horizontal irradiance as a function of the three illuminance measurements. The approximation performance of the regression is shown in Figure 5 resulting in a Mean Average Error (MAE) of 43.2 W/m^2 and an RMSE of 86.6 W/m^2. It is assumed that the regression model is also representative of other periods and reproduces the global horizontal irradiance with a reasonable accuracy.

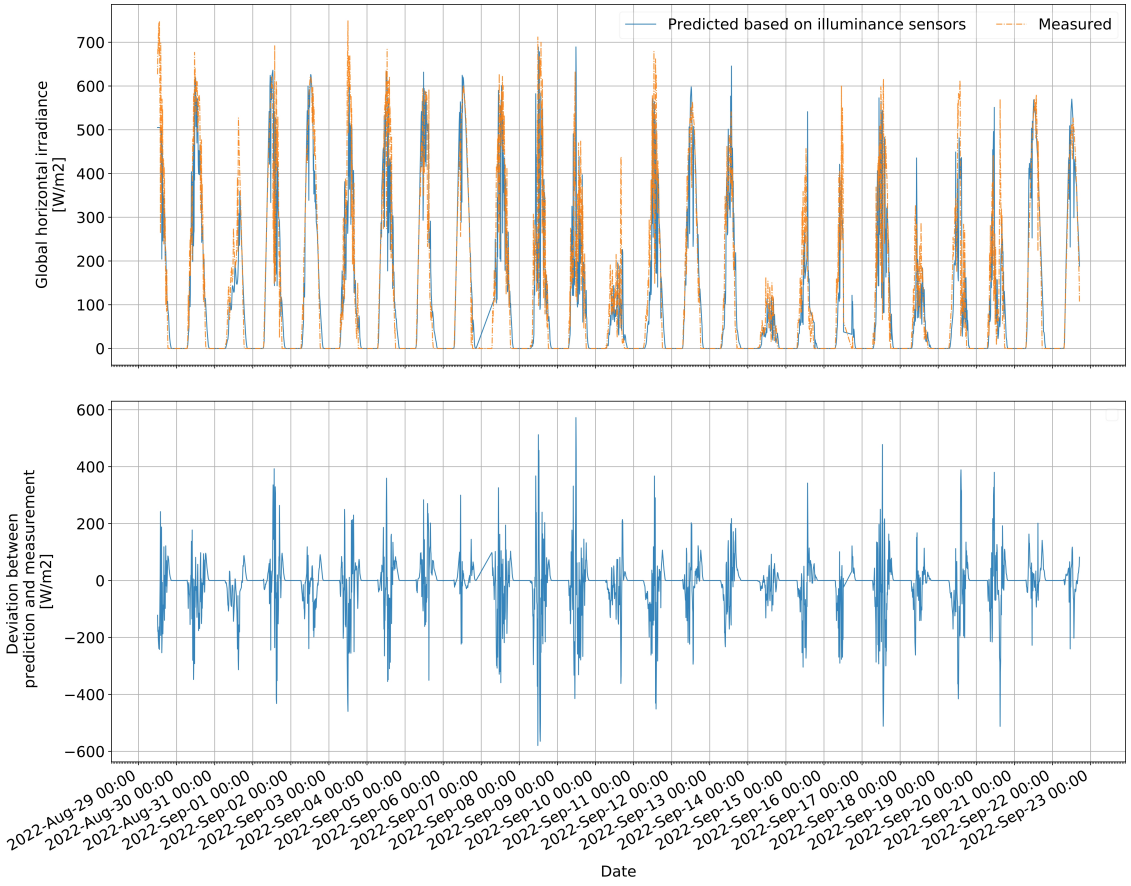

Figure 5: Regression of the global horizontal irradiance based on illuminance measurements: $ghi_{predicted} = 2.81\text{E-}3 \cdot illum_{south-west} + 1.93\text{E-}4 \cdot illum_{north-west} + 4.83\text{E-}3 \cdot illum_{south-east}$ (MAE: 43.2 W/m^2, RMSE = 86.6 W/m^2)

Real-time communication via MQTT

The MQTT protocol transfers MPC outputs (the control inputs to be implemented by the actuators) and the real-time sensor measurements from/to the cloud, where the MPC is executed. For this purpose, the Python package *paho-mqtt* is employed. The package enables communications via a coupled MQTT broker to publish messages (the control inputs, in this context referred to as *commands*) and to subscribe to topics (the sensor measurements, in this context referred to as *attributes*) and published messages. All data that are communicated via MQTT are stored in the CrateDB database. Before the start of the MPC execution, a subscription is undertaken for all room-relevant measurements and control inputs. The subscribed topics are formulated based on the mapped device IDs from the ETS described in the previous section. The same applies to the published topics, which contain the control inputs sent to the respective actuators and are based on mapping the Modelica variables onto the corresponding device IDs including a potential unit conversion.

State estimation

To initialize the optimization state variables based on the most recent measurements, state estimation is run before every MPC iteration. It enables to estimate the current value of non-measurable states such as the temperatures of walls or the fluid and solid components of the radiators and floor heating. Apart from this, state estimation can compensate for potential modeling or measurement errors. In this work, state estimation in the form of an Unscented Kalman Filter (UKF) based on *ukf.py* from the JModelica.org toolchain is applied. Its implementation is based on the work by Sun et al. [45] (non-augmented version described in this work) and Wan and Van Der Merwe [46]. A UKF is chosen due to its low computational requirements and real-time capabilities for estimating nonlinear systems. Input to the UKF estimator is the most recent room temperature measurement based on which all Modelica model states are calculated, which are used then to initialize the optimization problem of the next MPC iteration. The UKF performance can be adjusted by specifying process and measurement noise and, as a result, strengthen the confidence in either the measurements or the Modelica model.

Parameter estimation

For creating the MPC controller model, the first version of the office space model is created based on information derived from construction plans and available specifications of actuators and building envelope. The modeled room components comprise two radiators, the floor heating, the air volume, two pumps (one for the radiators and the floor heating each), three valves, three windows including Venetian blinds (based on the created model in [34]), an external and an internal adiabatic wall as well as occupancy. To calibrate the physics-based Modelica room model, an iterative, nonlinear parameter estimation is implemented based on *greybox.py* of the JModelica.org toolchain, Optimica [28] and IPOPT to estimate selected model parameters. The basic *greybox.py* submodule has been extended by a simulative sensitivity analysis determining the order of estimating the parameters and a division of the calibration horizon into periods focusing on specific physical phenomena. The input data for the parameter estimation are retrieved from the CrateDB and comprise measurements for the room temperature, heating and shading control inputs, weather-related data (from the building weather station), counted number of persons and heating water supply temperatures for the radiators and floor heating. In addition, a unit conversion from the KNX units towards the equivalent units in the Modelica model is performed.

The parameter estimation problem is solved over a user-defined time horizon minimizing the quadratic deviation between the measured and predicted room temperature (with t_0 and t_f as the start and final time of the prediction horizon):

$$\min_{p} \quad J = \int_{t_0}^{t_f} (y_{\text{measured}}(t) - y_{\text{optimized}}(t))^2 dt \tag{1a}$$

$$\text{s.t. } F(t, dx, x, u, w, p) = 0 \tag{1b}$$

$$x(t_0) = x_0 \tag{1c}$$

$$\underline{p}_i \leq p_i \leq \bar{p}_i \qquad \forall i \in \{1, \ldots, \text{n}\} \tag{1d}$$

Here, y_{measured} corresponds to the measured, $y_{\text{optimized}}$ to the optimized room temperature and p represents the vector of free parameters with size n. For every parameter to be calibrated, minimum and maximum bounds (Equation (1d)) as well as an initial guess can be specified. Equation (1b) describes the general nonlinear system DAEs.

The parameters that are selected by the user to be calibrated are iteratively estimated in an order established by a preceding simulative sensitivity analysis, which calculates the influence of the selected parameters on the room temperature dynamics. The most influential parameter is estimated first, while the remaining selected parameters are fixed to their initial guess. After the optimization, the cost function result is evaluated to analyze if the calibrated parameter can reduce the cost function compared to the previous parameter selection. If this applies, the parameter is kept in the total parameter set of free parameters that are estimated in the next iteration, otherwise, it is removed and fixed to its initial guess to reduce the degrees of freedom in the optimization problem. The procedure is repeated with the next most influential parameter, which is added to the total parameter set, and the estimation problem is solved again. The parameter estimation ends if all user-specified parameters have been evaluated. Currently, the parameter estimation is implemented in an offline configuration detached from the MPC, but it could be adapted to be run at regular intervals within an online MPC execution resulting in a continuously updated MPC model.

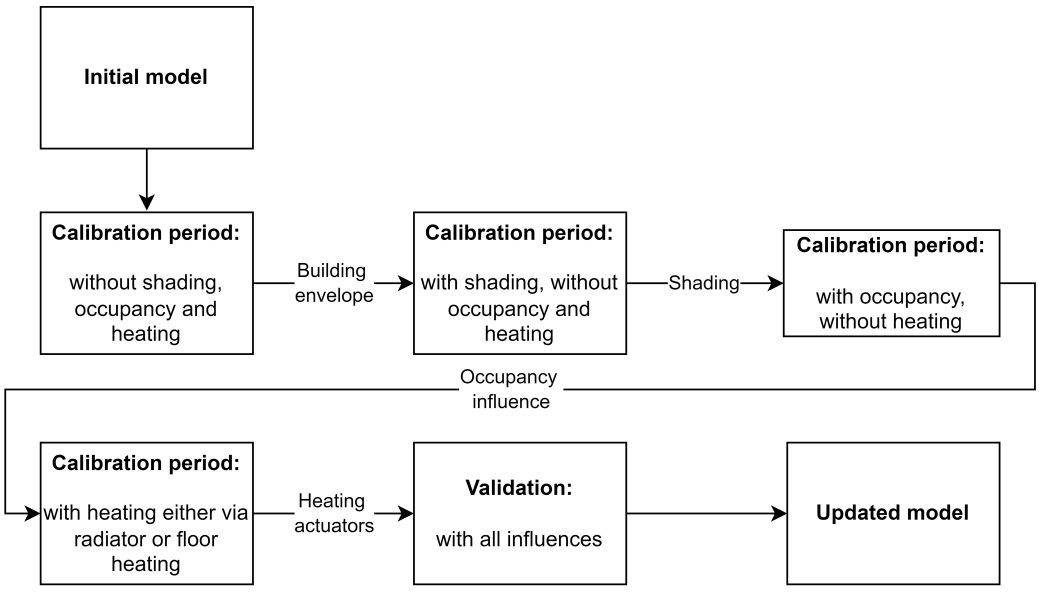

Figure 6: Iterative calibration process for estimating model parameters

To reduce the number of influencing factors that impact the measured room temperature during an estimation period and to be able to trace back dynamics in the measured temperature trajectory to a specific room component or physical phenomenon, different calibration periods are employed. In each calibration

period, the focus is set on a specific isolated influential factor (e.g., the building envelope, shading or heating systems) and the impact of other components is tried to be reduced. The sequence of the different calibration periods for the controlled office space is visualized in Figure 6. The boxes represent the individual calibration periods including focused and neglected influential factors and the outputs of the boxes constitute the components whose parameters have been calibrated. In the first period, the parameters of the building envelope are calibrated by focusing on periods without shading, occupancy and heating. The estimated parameters for the building envelope are set to fixed in the next calibration period, where the focus is set on the influence of the shading. This procedure continues for calibrating the parameters of the occupancy influence and finally, the isolated heating actuators in periods, where just one of the heating actuators is operated. In the final calibration, the building is exposed to all influential factors and disturbances validating the overall performance of the updated model to track the room temperature measurements. The respective calibration periods isolating specific physical phenomena or components are currently manually extracted from the total data set but could be automatically extracted based on a data filtering script in the future.

4. MPC formulation

In the conventional control mode, both for the radiators and the floor heating, a local PI-controller in the building regulates the respective valve openings based on the current room temperature and a temperature set-point provided by the occupant via an on-site room control panel. When applying the MPC mode, two different heating control modes are available. In the first MPC heating control mode, temperature set-points calculated by the MPC are sent to the local controllers and implemented by them. In the second control mode, which is pursued in the experimental MPC of this work, the controllers are deactivated by a blocking signal, and the valve openings are set directly by the MPC. The sent radiator valve opening applies to both radiators. When returning into the conventional control mode, the controllers are activated again. The communication with the two radiators is carried out via the wireless EnOcean protocol. The EnOcean actuators are configured to wake up every 10 minutes, receive the most recent control input and implement it. The other actuators are addressed via KNX.

The blinds on each facade can be individually controlled via the vertical shading position and the inclination angle as depicted in Figure 7. A wind sensor of the building weather station monitors wind speed and in case of exceeding a threshold of 10 m/s, all blinds are raised.

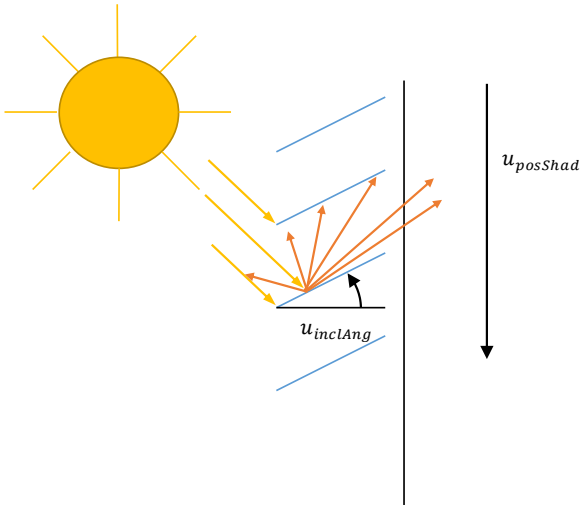

Figure 7: Venetian blinds (u_{inclAng}: inclination angle; u_{posShad}: shading position)

The optimization problem to be solved in every MPC iteration is formulated as follows (with t_0 and t_f as the start and final time of the MPC prediction horizon):

$$\min_{\substack{u_{\text{rad}},u_{\text{floorHeat}},\\ u_{\text{posShad},1},u_{\text{inclAng},1},\\ u_{\text{posShad},2},u_{\text{inclAng},2},\\ u_{\text{posShad},3},u_{\text{inclAng},3},\\ u_{\text{al}},\underline{\varepsilon},\bar{\varepsilon}}} J = \int_{t_0}^{t_f} (\alpha_{\text{rad}} \cdot \dot{m}_{\text{rad}}(t) \cdot (T_{\text{supply,rad}}(t) - T_{\text{return,rad}}(t))$$

$$+ \alpha_{\text{floorHeat}} \cdot \dot{m}_{\text{floorHeat}}(t) \cdot (T_{\text{supply,floorHeat}}(t) - T_{\text{return,floorHeat}}(t))$$
$$+ \delta \cdot \alpha_{\text{Light}} \cdot u_{\text{al}}(t) + \theta \cdot (\underline{\varepsilon}(t)^2 + \bar{\varepsilon}(t)^2)$$
$$+ \sigma_{\text{posShading}} \cdot \Delta u_{\text{posShad}}(t)^2 + \sigma_{\text{inclAng}} \cdot \Delta u_{\text{inclAng}}(t)^2) dt \tag{2a}$$

$$\text{s.t.} \quad F(t, dx, x, u, w, p) = 0 \tag{2b}$$
$$x(t_0) = x_0 \tag{2c}$$
$$\underline{T}_{\text{room,air}}(t) - \underline{\varepsilon}(t) \leq T_{\text{room,air}}(t) \leq \bar{T}_{\text{room,air}}(t) + \bar{\varepsilon}(t) \tag{2d}$$
$$\underline{\varepsilon}(t), \bar{\varepsilon}(t) \geq 0 \tag{2e}$$
$$illum_{\text{dl}}(t) + illum_{\text{al}}(t) \geq illum_{\text{set}}(t) \tag{2f}$$
$$u_{\text{rad,min}} \leq u_{\text{rad}} \leq u_{\text{rad,max}} \tag{2g}$$
$$u_{\text{floorHeat,min}} \leq u_{\text{floorHeat}} \leq u_{\text{floorHeat,max}} \tag{2h}$$
$$u_{\text{posShad,min}} \leq u_{\text{posShad,i}} \leq u_{\text{posShad,max}} \quad \forall i \in \{1,2,3\} \tag{2i}$$
$$u_{\text{inclAng,min}} \leq u_{\text{inclAng,i}} \leq u_{\text{inclAng,max}} \quad \forall i \in \{1,2,3\} \tag{2j}$$

In these formulations, u_{rad} and $u_{\text{floorHeat}}$ correspond to the valve openings of the radiators and floor heating (in %). $u_{\text{posShad,i}}$ and $u_{\text{inclAng,i}}$ with $i \in \{1,2,3\}$ are the vertical shading position and inclination angle of the respective window facade. i=1 corresponds to the south-east, i=2 to the south-west and i=3 to the north-west facade. $\underline{\varepsilon}$ and $\bar{\varepsilon}$ are introduced slack variables softening the thermal comfort constraint (Equations (2d) and (2e)). u_{al} is the theoretical control input for artificial lighting, which is assumed to vary linearly with the generated artificial illuminance $illum_{\text{al}}$, which is calculated based on the calculated $illum_{\text{dl}}$ from the model. α_{rad} and $\alpha_{\text{floorHeat}}$ are energy weighting factors for the radiators and floor heating consisting of the heat capacity of water, α_{Light} is a weighting factor for the energy consumption of artificial lighting and θ a factor penalizing room temperatures outside the comfort range. $\dot{m}_{\text{rad}}$ and $\dot{m}_{\text{floorHeat}}$ are the total heating water mass flows supplied to the radiators and floor heating. $\underline{T}_{\text{room,air}}$ and $\bar{T}_{\text{room,air}}$ are the time-variant lower and upper comfort temperature bounds. $T_{\text{supply,rad}}$, $T_{\text{return,rad}}$, $T_{\text{supply,floorHeat}}$ and $T_{\text{return,floorHeat}}$ are the supply and return water temperatures of the radiators and floor heating. $illum_{\text{dl}}$ is the daylight illuminance transmitted by windows and Venetian blinds, $illum_{\text{al}}$ the artificial light illuminance and $illum_{\text{set}}$ the time-variant minimum comfort illuminance. Equation (2b) describes the general nonlinear DAEs. Equations (2g) to (2j) represent the minimum and maximum bounds for the control inputs with $u_{\text{posShad,i}} \in [0, 1]$ (0: fully opened, 1: closed) and $u_{\text{inclAng,i}} \in [0°, 90°]$ (0°: fully opened, 90°: closed).

The first two terms of the cost function (Equation (2a)) represent the heating power consumption of the radiators and the floor heating. The third term contains the electrical power consumption for the artificial lighting extended by the factor δ to optionally put more weight on the transmission of daylight into the room. The fourth term corresponds to the thermal discomfort in the form of the quadratically penalized slack variables $\underline{\varepsilon}$ and $\bar{\varepsilon}$ and the two last terms penalize the change in the shading control inputs based on $\sigma_{\text{posShading}}$ and σ_{inclAng} to avoid oscillatory, user-disturbing operation. The factors δ, θ, $\sigma_{\text{posShading}}$ and σ_{inclAng} could also serve as tuning parameters (in combination with the comfort bounds), which are adjusted by the occupants over time to maximize user satisfaction with the implemented building control with regard to energy efficiency, daylight transmission, thermal discomfort and shading frequency according to Figure 8. In the current version, the weighting factors were specified based on initial guesses and adjusted after evaluation of first control results.

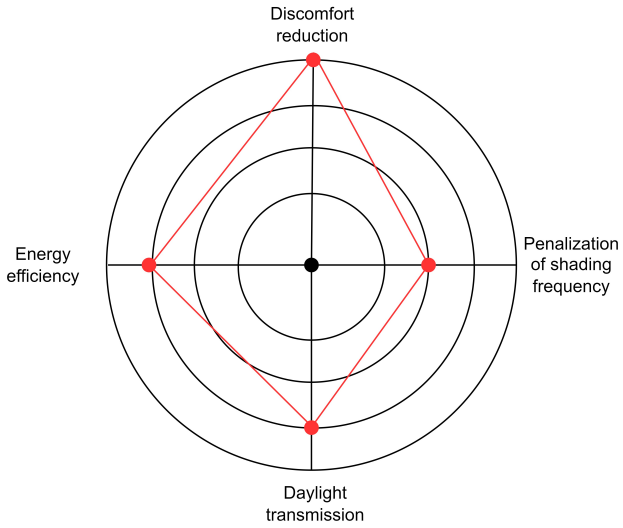

Figure 8: Adjustability of the weighting of the cost function terms

Both thermal and visual comfort are considered within the optimization constraints. The bounds for the room temperature comfort ($\underline{T}_{\mathrm{room,air}}$ and $\bar{T}_{\mathrm{room,air}}$) and the minimum illuminance ($illum_{\mathrm{set}}$) are set according to daytime. From 8 a.m. to 5 p.m. (times of potential occupancy), the minimum and maximum bounds for the comfort temperature are 21 and 23 °C, outside these times the comfort range is widened to 19–26 °C, as no specific comfort requirements need to be fulfilled there. With regard to visual comfort, a minimum illuminance of 500 Lux [47] has to be fulfilled during occupied times (8 a.m.–5 p.m.) by the combination of natural daylight and artificial illumination. In the current configuration, temperature set-points entered by the occupants via the room control panel are not considered or integrated into the MPC as new comfort bounds, which is planned for future versions. In case the occupants manually operate the shading via the room control panel, the MPC gets feedback (by comparing the control input sent in the previous MPC iteration and the current feedback) and does not send any shading control input for two hours. Apart from this, MPC control inputs for the shading that deviate less than 5 % from the previously sent value are filtered to reduce disturbances to the occupants. The prediction horizon of the MPC is 24 h and the sampling period is 15 min. The toolchain is run on an OpenStack virtual machine with Ubuntu 18.04, 8 VCPUs and 32 GB RAM.

5. Results

5.1. Parameter estimation

The prediction horizon of the parameter estimation is set to 24 h. The start time of the parameter estimation is always set to 00:00 (12 a.m.) on each day to facilitate the initialization of the model state variables. It is assumed that at 00:00 all heating systems have not been activated for a longer period due to a lower minimum temperature during the night and the corresponding capacitances (the fluid and solid components of the radiators and floor heating) have converged to an equilibrium temperature, which is identical to the measured room temperature at this time.

The parameter estimation was carried out with data from September 17 to November 4, 2022. In Figure 9 the parameter estimation results based on the final parameter set are shown for a calibration period in which the room temperature is impacted by all potential influential factors (October 26, 2022). On this day, the building is affected by heating via radiators (second subplot) and floor heating (third subplot), shading (fourth subplot) and a few occupants (sixth subplot). The "Irradiance" subplot reveals a high amount of

direct solar irradiance hitting the window facades of the room. The "Room temperature" subplot shows a good approximation of the measured room temperature by the estimated one. This applies to both the optimized (resulting from the optimization solver IPOPT) and the simulated trajectory (FMU simulation based on the estimated parameters). The impact of the second peak of the direct solar irradiance (around 12:00) on the room temperature is slightly overestimated in the model. The RMSE between the measured and estimated simulated room temperature trajectory is 0.31 K. It should be noted that the global horizontal irradiance (as well as the direct and diffuse irradiance) depicted in the last subplot is not completely measured but calculated based on the external illuminance measurements and the evaluated regression function.

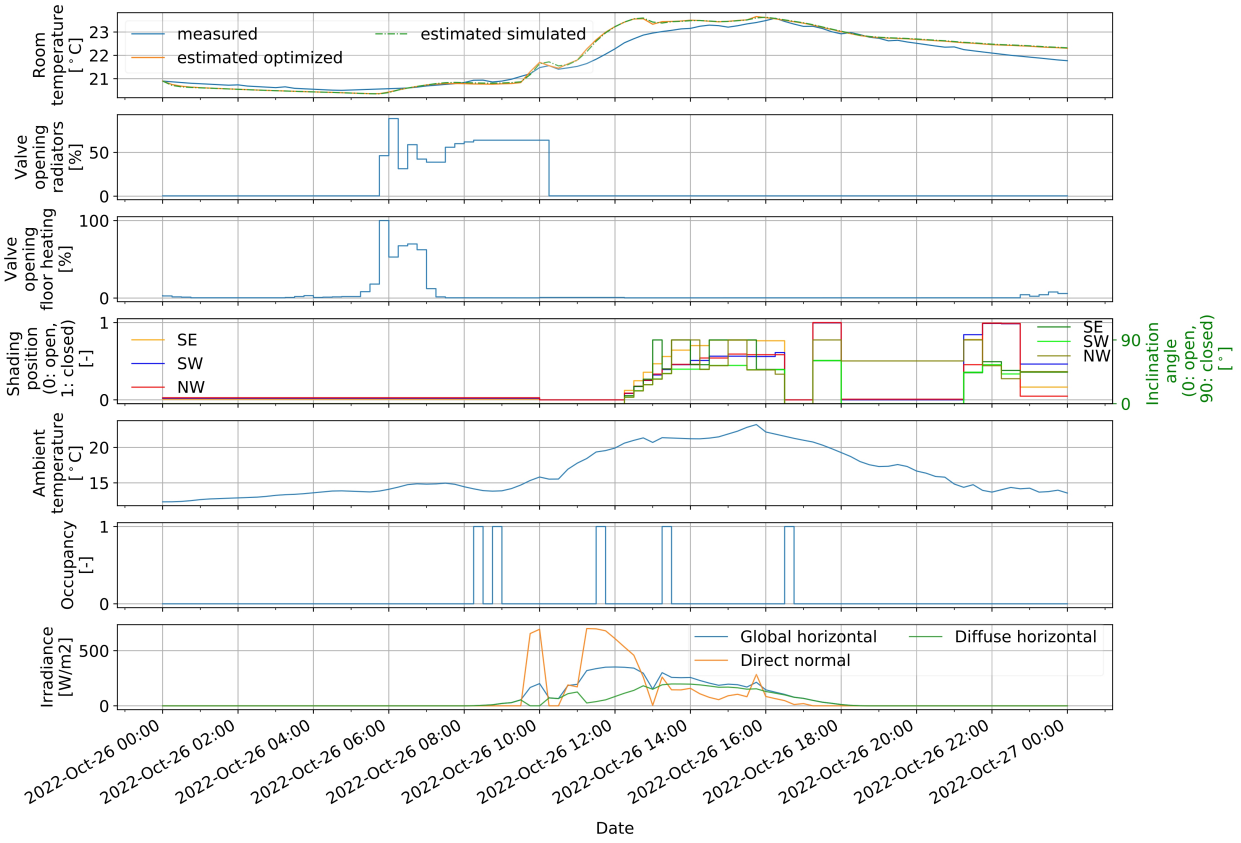

Figure 9: Parameter estimation results for an exemplary calibration period with all influences

For the final set of estimated parameters, the RMSE between the measured and estimated simulated room temperature trajectory averaged over all considered calibration periods from September 17 to November 4, 2022 is 0.49 K. According to Blum et al. [19], an RMSE for approximating the building envelope below 1 K is an indicator of sufficient model accuracy for use in building MPC. Hence, in this work, a high model accuracy is achieved by the combination of the Modelica model generation and the refining parameter estimation.

5.2. MPC

The MPC was experimentally applied to the laboratory room for 21 days from October 21 to November 11, 2022. During that period, the MPC was stopped and reinitialized at some points to update the calibrated room model or adjust parameters in the weather forecast or weighting factors of the cost function. The results for the entire controlled period retrieved from the database are plotted in Figure 10 and in a higher temporal resolution for November 7 to 11 in Figure 11.

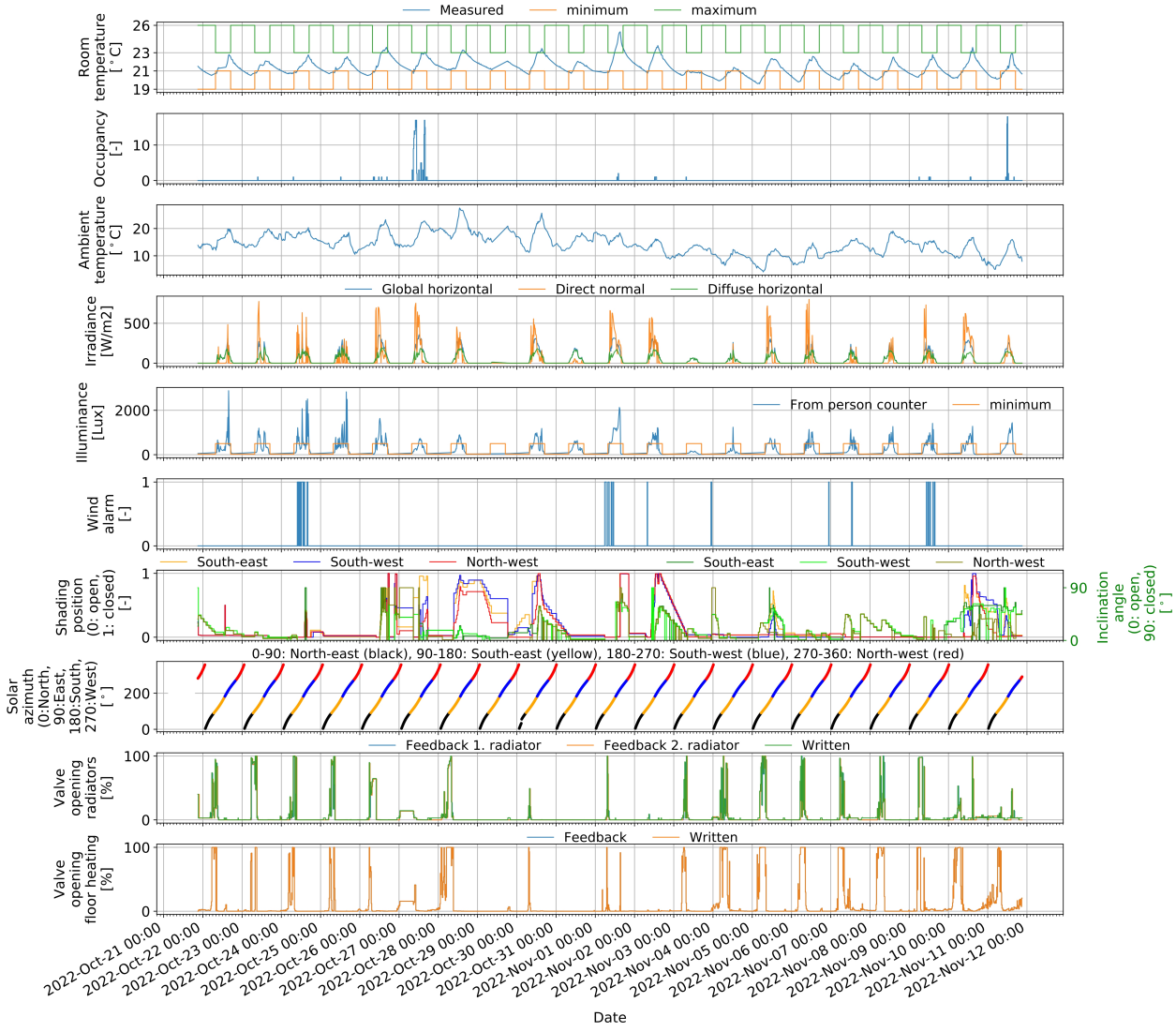

Figure 10: Experimental MPC on the JuLab from October 21 to November 11, 2022

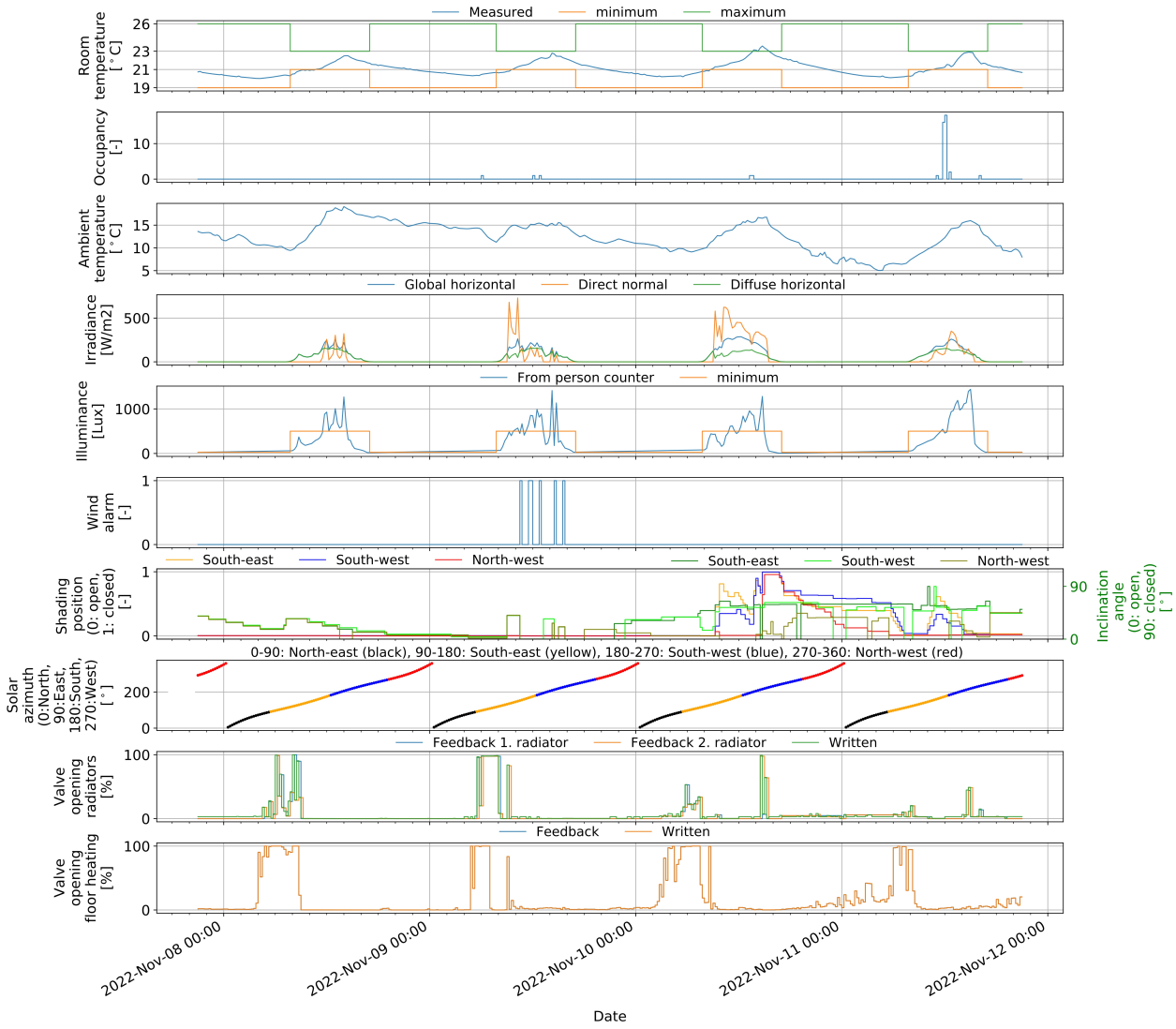

Figure 11: Experimental MPC results from November 7 to 11, 2022 (thermal discomfort of 0.64 Kh/d)

The first subplot depicts the measured room temperature and the specified time-varying minimum and maximum comfort bounds including the widened comfort range during unoccupied periods (night setback, from 5 p.m.–8 a.m.). The second, third and fourth subplot show the disturbance quantities that have an influence on the room dynamics. The "Occupancy" subplot exhibits little occupancy on some days, whereas, most of the time, the room is not occupied. The "Ambient temperature" subplot reveals a warmer first period (October 21 to November 2) with ambient temperatures near 20 °C followed by colder temperatures near 10 °C (November 3 to 11). The "Irradiance" subplot shows the irradiance quantities of the global horizontal, direct normal and diffuse horizontal irradiance, which are calculated based on the external illuminance measurements. On October 26, 27, 28 and 30 as well as November 1, 2, 5, 10 and 11, there is an increased amount of direct irradiance. The "Illuminance" subplot depicts the indoor room illuminance measured by the person counter and the minimum comfort illuminance specified in the optimization (to be fulfilled by the sum of daylight and artificial lighting). In the "Wind alarm" subplot, the exceedance of the wind speed threshold is indicated, which causes a wind alarm and raise of all Venetian blinds to avoid damage. The "Shading position" subplot depicts the shading feedback for all window facades, both for the vertical shading position (left y-axis) and the inclination angle (right y-axis). For more detailed information about the current solar position, the solar azimuth is shown in the "Solar azimuth" subplot. By the color of the respective marker, the facade that is mainly irradiated at this time can be derived. The facade colors correspond to the ones of the shading position in the "Shading position" subplot. In the last two subplots, the manipulated valve openings for the radiators and floor heating are shown. The sent radiator valve opening applies to both radiators but may be realized by the radiators at different times. Both the written and measured feedback values are outlined. For the floor heating, these trajectories generally coincide, for the radiators, there is a slight time delay due to the wireless EnOcean communication and described on/off behavior (visible in Figure 11).

Since the building is solely equipped with building-wide energy consumption meters, a quantified evaluation of the energy efficiency of the MPC approach in comparison to a conventional control is currently not possible. Nevertheless, the first subplot of Figure 10 insinuates the energy efficiency of the MPC approach by showing a heating control, which tries to operate the room temperature near the lower comfort bounds. The night setback is exploited and, in the case of heating demand, the room is preheated to reach the minimal comfort bound of 21 °C at 8 a.m. of the next morning, which is the time when the building is prepared for potential occupants. For most days, the minimum comfort temperature at this time is reached. On November 4, 7, 9 and 11, the minimum comfort bound is slightly exceeded. From Figure 12, which compares forecasted and measured disturbance trajectories, it can be observed that during the morning hours on November 4, 9 and 11, the forecasted ambient temperature is approximately 2 °C higher than the measured one, which could contribute to explaining the exceedance. On November 3, the heat gains in the room are overestimated in the MPC to some degree, which leads to small exceedance of the lower comfort bound during most of the day. It should be noted that thermal comfort is not considered a hard constraint but softened and penalized in the cost function according to Equation (2a) and Equation (2d). This allows certain discomfort according to the weighting of the cost function terms and the balance between energy efficiency and discomfort minimization.

Due to its higher inertia, the floor heating is generally activated earlier and operated for longer times compared to the radiators (visible in Figure 11). Moreover, the floor heating is controlled in a less dynamic and oscillating way compared to the radiators. Consequently, the floor heating covers the base load exploiting the higher energy efficiency due to lower supply temperatures, while the radiators compensate for peak loads. After reaching the minimum comfort temperature in the morning and for most of the occupancy period (8 a.m.–5 p.m.), the heating systems are generally not activated. For the ambient temperatures during the controlled period, the daily heat gains (especially solar irradiance) are sufficient to keep the room temperature above its minimum bound during the day.

The three separately controlled Venetian blinds attempt to predictively keep the room temperature near the upper comfort bound while harvesting a maximum of the solar heat gains and daylight to reduce energy consumption for heating and lighting. Shading is operated on October 26, 27, 28 and 30 as well as November 2, 5, 10 and 11. The north-west facade is generally shaded to a lower extent compared to the south-east and south-west facades, since the sun is only shining on this facade during the afternoon (observable in

the "Solar azimuth" subplot). Hence, this window facade can be used to transmit daylight, while, on days with high direct solar irradiance, mainly the two south-oriented facades are shaded to a higher extent. On some days with shading, there is a slight exceedance of the upper comfort bound (e.g., on October 26, 28 and 30 and November 10), but, in general, the shading control shows a satisfactory performance. On November 2, the forecasted direct normal irradiance is underestimated due to a maximum threshold for the solar zenith angle in the DIRINT model (equivalent to the neglect of any direct irradiance, where the solar zenith angle is above this threshold), which was set too low with a value of 65°. The underestimation of the direct normal irradiance on this day is also detectable in Figure 12. This leads to the calculation of a very low amount of direct normal irradiance on days with a small solar elevation. After this day, the parameter was corrected to a value of 80°. Generally, the shading control tries to avoid an oscillatory, user-disturbing operation (according to Equation (2a); especially weighted for the vertical shading position due to the higher disturbance potential compared to the inclination angle) and smoothly increases or decreases the shading position for most days. The apparent oscillations for the inclination angle (frequent switching to an inclination angle of 0°) can be explained by the motion sequence that is performed if the vertical shading position is changed. For changing the shading position, the blinds have to switch to an inclination angle of 0°, move to the new vertical shading position set-point and restore the old inclination angle. The blinds are raised on days during which there is no risk to exceed the upper comfort bound to maximize the transmission of solar heat gains and daylight. The "Illuminance" subplot exhibits that during most of the controlled period in the daytime (also during times without occupancy and artificial lighting), the minimum illuminance of 500 Lux is fulfilled.

On November 1, the shading could not be controlled by the MPC due to too high wind speeds, which resulted in an automatic raise of all blinds (indicated in the "Wind alarm" subplot). On this day with high direct irradiance, the upper comfort bound is significantly exceeded (by more than 2 °C), which highlights the relevance of (predictive) shading control for preventing overheating. Moreover, the time delay between the peaks of the solar radiation (around 12 p.m.) and the room temperature (around 3 p.m.) is shown, which is attributed to the solar heating of the room surfaces, which heat up the room air temporally delayed.

On October 29, the MQTT broker crashed, which caused a communication loss from approximately 9 a.m. to 6 p.m. The shown results are interpolated between these times (straight lines visible in the "Room temperature" and "Ambient temperatures" subplots).

In Figure 12 the forecasted and measured disturbance quantities for the ambient temperature and the solar irradiance quantities (global horizontal, direct normal and diffuse horizontal) are compared. The forecasted disturbance data are used in the optimization and are logged from October 24 on. The measurements are based on the sensors of the local weather station on the roof of the building. It should be noted that the "measured" trajectories for the irradiance quantities are calculated based on the external illuminance measurements as described in the previous sections. The first subplot depicts the measured and forecasted ambient temperature. In general, the trend and dynamics of the forecasted ambient temperature are in agreement with the measured trajectory. However, peaks (both negative and positive) are often underestimated (for positive peaks on e.g., October 26, 28, 30 and November 6, 8 and 10; for negative peaks on November 4, 5, 6, 8, 9 and 11). The forecast errors range up to 2 °C for the negative peaks and complicate the predictive preheating to reach the minimum comfort bound at the beginning of the occupancy (8 a.m.). The RMSE between the measured and forecasted ambient temperature is 1.31 K.

The second subplot reveals the measured and forecasted trajectories for the global horizontal irradiance. The trajectories show a good agreement throughout the control horizon with an RMSE of 48.2 W/m^2 (on October 29, the MQTT communication loss is visible). In the third subplot, the trajectories for the direct normal irradiance are shown, which exhibit larger deviations. This can be partly traced back to the threshold for the maximum zenith angle, which was set too low in the DIRINT model until November 2 (especially evident on November 1 and 2). These forecast errors also manifest themselves in the last subplot of the diffuse horizontal irradiance, where the forecast accuracy is significantly increased after this day. After November 2, on some days, the direct normal irradiance is forecasted well (November 8, 9 and 10), on other days it is overestimated (November 5 and 11) or underestimated (November 6). The RMSE between the forecasted and measured trajectories is 126.6 W/m^2 for the direct normal and 48.9 W/m^2 for the diffuse horizontal irradiance.

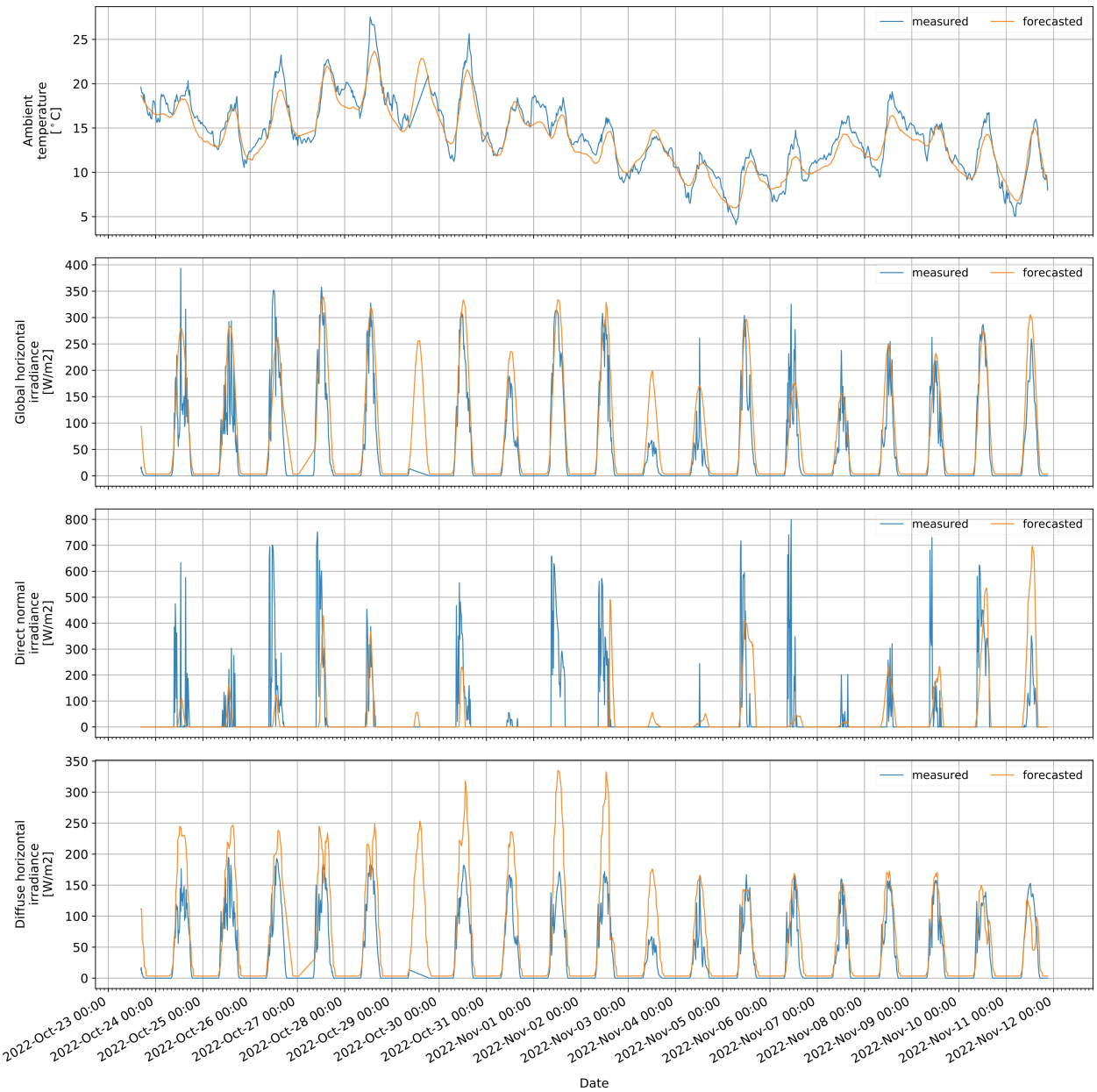

Figure 12: Comparison of forecasted and measured disturbances

The total discomfort averaged over the entire MPC execution period (adjusted for November 1, where shading operation was not possible) is 0.53 Kh/d. This reveals that there is still room for improvement if the full focus should be put on discomfort minimization. The specification of the different weighting factors of the cost function terms (energy efficiency, discomfort minimization, daylight transmission and penalization of shading oscillation) should be evaluated carefully and adjusted to occupancy preferences. Against the background that the room control is very sensitive to the direct normal irradiance due to its large window facades, the forecast accuracy of this irradiance quantity and potential improvements (e.g. the use of the forecasted cloud cover to refine the forecast) should be investigated further. In analogy with the described occupancy correction step, the irradiance (and ambient temperature) forecasts for the next sampling period could be corrected or adjusted based on current measurements.

5.3. RBC

To place the control performance of the MPC and allow further conclusions on its control quality, a conventional reference control in the form of a combined RBC+PI-control was run over a similar period of an equal horizon of 21 days. The reference control was executed from April 3 to April 24, 2023, which constitutes a period with similar disturbance quantities of ambient temperature, solar radiation and occupancy level. The control performance and disturbance quantities are exhibited in Figure 13. Compared to the ambient temperatures during the MPC execution, the ambient temperatures are lower (average ambient temperature during MPC: 14.2 °C; during RBC: 9.7 °C). As described for the conventional control mode, the valve openings of the floor heating and radiators are controlled by the locally implemented, conventional PI-controllers that track a room temperature set-point of 21 °C, which is sent by the cloud and equivalent to the lower MPC bound during the occupied periods. The Venetian blinds are operated in a rule-based manner based on a script running in the cloud, which is meant to mimic a conventional shading control. Shading is operated, if the room is not occupied, based on an external illuminance sensor mounted on the roof of the building. If the illuminance measurement exceeds a threshold of 50 klx, the blinds of the current irradiated facade are lowered and inclined to an intermediate inclination angle of 60°.

In general, the conventional control demonstrates good control quality by preserving thermal comfort for most of the time horizon. This results in a total averaged discomfort of 0.47 Kh/d, which is adjusted for periods with wind alarm or occupancy, since during these times, the shading was not operated. On April 22, there was a failure in the MQTT communication, which is why this day is not accounted for in the discomfort calculation. The overall discomfort level is similar to the one in the MPC. The last two subplots reveal a rather inert configuration of the PI-controllers tracking the room temperature. The valve openings are opened if the room temperature falls below 21 °C, but the openings are increased very slowly. Thereby, during nights and also at several beginnings of the occupancy periods at 8 a.m., the room temperature falls below 21 °C leading to some discomfort (e.g., on April 12, 16, 19 and 20). Nevertheless, the nightly decrease of the temperatures is not as large as in the MPC. Operating the heating actuators already during the evening (e.g., on April 6), when the potential occupants enter the room 14 hours later, suggests a rather energy-inefficient behavior. Due to their inert configuration, the PI-controllers keep the valve openings open from falling below 21 °C till reaching a temperature of approximately 21.5 °C (e.g., visible on April 7), which equally constitutes energy-inefficient control. The floor heating and radiators are activated at the same time but the valve opening of the radiators is increased to a higher extent. A distribution of the heat load into a base and peak load is not visible, e.g. by activating the floor heating earlier and for a longer time compared to the radiators, which would also exploit the higher energy efficiency of the floor heating due to lower supply temperatures. The control performance of the shading demonstrates good results for most of the time horizon. The upper comfort bound is exceeded on some days (April 5, 9, 14 and 21). On some days (April 12, 18, 19, 20 and 23), the shading is operated without fully exploiting the upper comfort bound and thereby, increases the demand for heating and lighting energy. This diverging shading behavior is expected to arise more often for varying ambient temperatures, as, depending on the thermal transfer between the room and the environment (as well as internal heat gains), the shading would be operated exceeding the upper comfort bound (on warmer days) or without exploiting the upper comfort bound (on colder days).

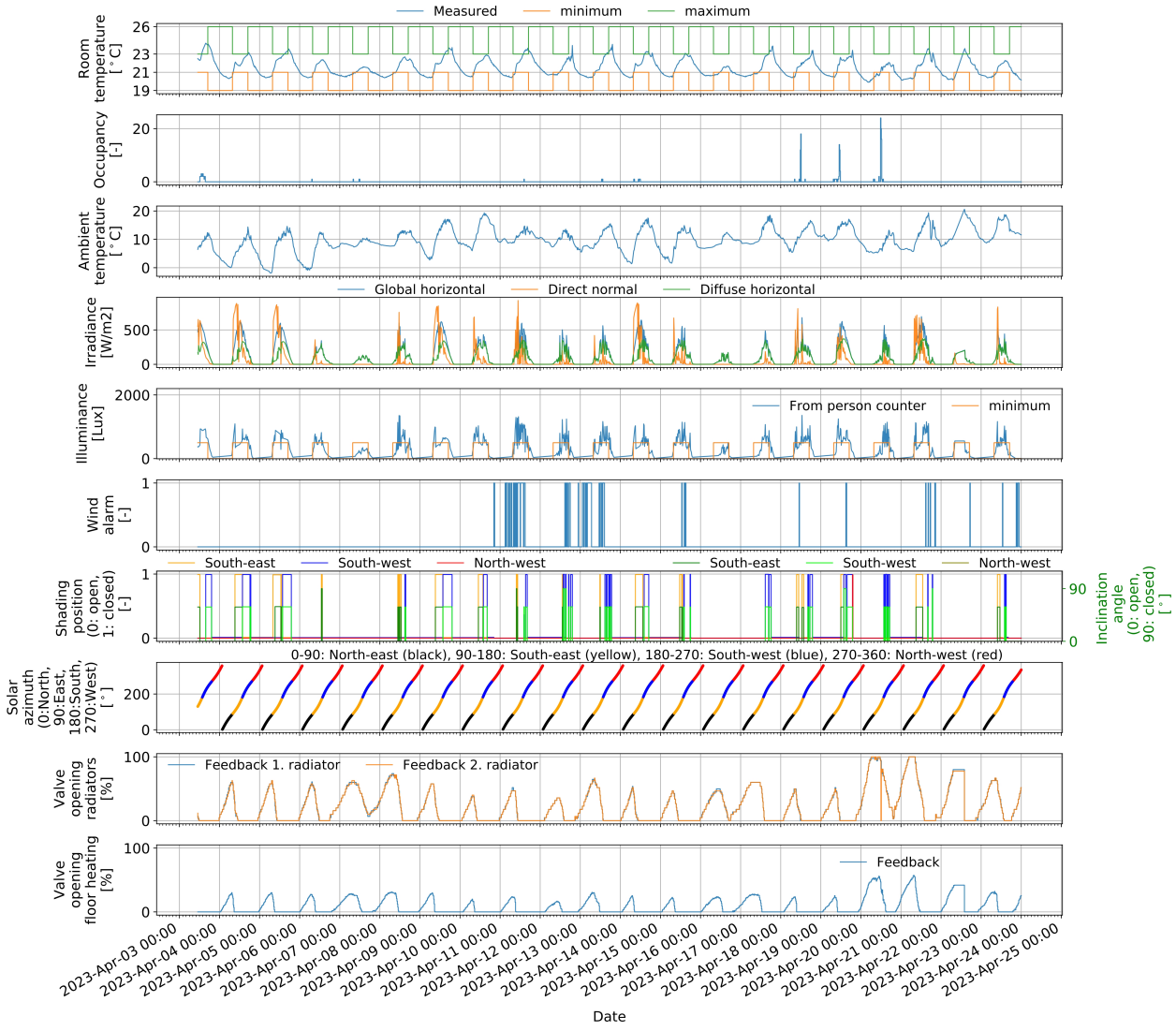

Figure 13: Combined RBC+PI-control on the JuLab from April 3 to 24, 2023

6. Conclusion and outlook

This work presents a field demonstration of a nonlinear, Modelica-based MPC applied to an HVAC system of an office space. The implemented MPC toolchain comprises state estimation, a forecasting module (for occupancy, supply temperatures and weather including calculation of direct and diffuse solar irradiance), parameter estimation and MQTT communication to actuators and sensors.

A nonlinear, iterative parameter estimation is performed before and during the MPC execution to calibrate selected parameters of the physics-based building model. The calibration is divided into separate periods that isolate the different heating flows influencing the room temperature (e.g., focus on the building envelope, shading or the heating actuators). The final calibrated model demonstrates a good high model accuracy and suitability for building MPC use with an RMSE between the measured and estimated room temperature of 0.49 K (averaged over all considered calibration periods from September 17 to November 4, 2022).

The experimental MPC was run for 21 days from October 21 to November 11, 2022 and included both operation of heating (manipulating the valve openings of radiators and floor heating) and shading (manipulating the shading position and inclination angle of three Venetian blinds). The MPC algorithm takes into consideration energy consumption for heating and lighting, thermal discomfort and potential shading disturbance to the occupants. The field test results manifest the capability of the MPC to maintain the room temperature largely within the comfort bounds. The heating and shading systems are controlled in an anticipatory manner to preserve thermal comfort while at the same time exploiting the widened comfort range during unoccupied periods. A room-individual energy consumption metering is currently not implemented, which would allow quantified conclusions with regard to the energy efficiency of the MPC in comparison to a conventional control. Nevertheless, the results demonstrate a heating control that operates the room temperature in an energy-efficient manner near the lower temperature bounds, exploits the higher energy efficiency of the floor heating and heats the actuators according to their dynamics to provide thermal comfort at the beginning of the occupancy periods. The shading control aims to exploit a maximum of the solar heat gains and daylight to minimize energy consumption for heating and lighting while considering the upper comfort bound, the different orientations of the window facades and potential disturbance to the occupants. Comparing the forecasted and measured disturbance quantities, sufficient forecast accuracy is revealed for all quantities with a potential for improvement for ambient temperature and direct normal irradiance. A comparison with a conventional control approach reveals the energy saving potentials of the MPC. The MPC operation results in a thermal discomfort of 0.53 Kh/d (averaged over the MPC execution period), which still gives room to general refinements or readjustments of the weighting factors in the cost function.

In future works, developed distributed [34], hierarchical [33] or hybrid [35] MPC approaches should be tested in field tests on the controlled room or larger buildings including integer decision variables. Air quality (e.g., in the form of CO_2) could be integrated as a comfort parameter based on the control of AHU models and components of the energy storage and supply (e.g., heat pumps) should be included in the control domain. The controlled room should be equipped with room-individual energy consumption metering to allow evaluation of the energy efficiency of MPC compared to a conventional PI control/RBC. Apart from the controlled heating water mass flows, supply temperatures should be added as control inputs providing more degrees of freedom within the optimization problem. The proposed control approach should be tested during different seasons and for more regular occupancy and user interactions integrating the user inputs into the MPC.

Author contributions

Maximilian Mork: Conceptualization, Methodology, Software, Investigation, Writing - Original draft, Writing - Review & Editing, Visualization. Florian Redder: Software, Resources, Data curation, Writing - Review & Editing, Visualization. André Xhonneux: Supervision, Writing - review & editing, Project administration, Funding acquisition, Resources. Dirk Müller: Supervision, Writing - review & editing, Project administration, Funding acquisition, Resources.

Declaration of competing interest

The authors declare that they have no known competing financial interests or personal relationships that could have appeared to influence the work reported in this paper.

Acknowledgments

The authors would like to thank their colleagues from the technical operations department for their support and feedback, in particular, Sebastian Neitzel and Andre Kleinen. Funding: This work was supported by the BMWK (Federal Ministry for Economic Affairs and Climate Action), promotional reference 03EGB0010A.

References

[1] United Nations Environment Programme, 2021 Global Status Report for Buildings and Construction: Towards a Zero-emission, Efficient and Resilient Buildings and Construction Sector, 2021. URL: https://globalabc.org/resources/publications/2021-global-status-report-buildings-and-construction.

[2] International Energy Agency, Building Energy Performance Metrics- Supporting Energy Efficiency Progress in Major Economies, 2015. URL: https://www.iea.org/reports/building-energy-performance-metrics.

[3] A. Afram, F. Janabi-Sharifi, Theory and applications of HVAC control systems - A review of model predictive control (MPC), Build. Environ. 72 (2014) 343–355. doi:10.1016/j.buildenv.2013.11.016.

[4] P. Höppe, Different aspects of assessing indoor and outdoor thermal comfort, Energy Build. 34 (2002) 661–665. doi:10.1016/S0378-7788(02)00017-8.

[5] G. Serale, M. Fiorentini, A. Capozzoli, D. Bernardini, A. Bemporad, Model Predictive Control (MPC) for enhancing building and HVAC system energy efficiency: Problem formulation, applications and opportunities, Energies 11 (2018). doi:10.3390/en11030631.

[6] T. Hilliard, M. Kavgic, L. Swan, Model predictive control for commercial buildings: trends and opportunities, Adv. Build. Energy Res. 10 (2016) 172–190. doi:10.1080/17512549.2015.1079240.

[7] M. Kavgic, T. Hilliard, L. Swan, Opportunities for implementation of MPC in commercial buildings, Energy Procedia 78 (2015) 2148–2153. doi:10.1016/j.egypro.2015.11.300.

[8] J. Cigler, D. Gyalistras, J. Siroky, V.-N. Tiet, L. Ferkl, Beyond Theory: the Challenge of Implementing Model Predictive Control in Buildings, in: 11th REHVA world Congr. 8th Int. Conf. Energy Effic. Smart Heal. Build., 2013, pp. 1008–1018.

[9] Y. Ma, A. Kelman, A. Daly, F. Borrelli, Predictive control for energy efficient buildings with thermal storage: Modeling, stimulation, and experiments, IEEE Control Syst. 32 (2012) 44–64. doi:10.1109/MCS.2011.2172532.

[10] S. C. Bengea, A. D. Kelman, F. Borrelli, R. Taylor, S. Narayanan, Implementation of model predictive control for an HVAC system in a mid-size commercial building, HVAC R Res. 20 (2014) 121–135. doi:10.1080/10789669.2013.834781.

[11] Z. Váňa, J. Cigler, J. Široký, E. Žáčeková, L. Ferkl, Model-based energy efficient control applied to an office building, J. Process Control 24 (2014) 790–797. doi:10.1016/j.jprocont.2014.01.016.

[12] S. R. West, J. K. Ward, J. Wall, Trial results from a model predictive control and optimisation system for commercial building HVAC, Energy Build. 72 (2014) 271–279. doi:10.1016/j.enbuild.2013.12.037.

[13] R. De Coninck, L. Helsen, Practical implementation and evaluation of model predictive control for an office building in Brussels, Energy Build. 111 (2016) 290–298. doi:10.1016/j.enbuild.2015.11.014.

[14] X. Pang, C. Duarte, P. Haves, F. Chuang, Testing and demonstration of model predictive control applied to a radiant slab cooling system in a building test facility, Energy Build. 172 (2018) 432–441. doi:10.1016/j.enbuild.2018.05.013.

[15] R. Carli, G. Cavone, S. Ben Othman, M. Dotoli, IoT Based Architecture for Model Predictive Control of HVAC Systems in Smart Buildings, Sensors 20 (2020) 781. doi:10.3390/s20030781.

[16] S. Yang, M. P. Wan, B. F. Ng, S. Dubey, G. P. Henze, W. Chen, K. Baskaran, Model predictive control for integrated control of air-conditioning and mechanical ventilation, lighting and shading systems, Appl. Energy 297 (2021) 117112. doi:10.1016/j.apenergy.2021.117112.

[17] J. Drgoňa, D. Picard, L. Helsen, Cloud-based implementation of white-box model predictive control for a GEOTABS office building: A field test demonstration, J. Process Control 88 (2020) 63–77. doi:10.1016/j.jprocont.2020.02.007.

[18] S. Freund, G. Schmitz, Implementation of model predictive control in a large-sized, low-energy office building, Build. Environ. 197 (2021) 107830. doi:10.1016/j.buildenv.2021.107830.

[19] D. Blum, Z. Wang, C. Weyandt, D. Kim, M. Wetter, T. Hong, M. A. Piette, Field demonstration and implementation analysis of model predictive control in an office HVAC system, Appl. Energy 318 (2022) 119104. doi:10.1016/j.apenergy.2022.119104.

[20] B. Merema, D. Saelens, H. Breesch, Demonstration of an MPC framework for all-air systems in non-residential buildings, Build. Environ. 217 (2022) 109053. doi:10.1016/j.buildenv.2022.109053.

[21] D. Sturzenegger, D. Gyalistras, V. Semeraro, M. Morari, R. S. Smith, BRCM Matlab Toolbox: Model generation for model predictive building control, in: 2014 Am. Control Conf., IEEE, 2014, pp. 1063–1069. doi:10.1109/ACC.2014.6858967.

[22] S. E. Mattsson, H. Elmqvist, Modelica - An International Effort to Design the Next Generation Modeling Language, IFAC Proc. Vol. 30 (1997) 151–155. doi:10.1016/s1474-6670(17)43628-7.

[23] M. Wetter, C. Van Treeck, New Generation Computational Tools for Building and Community Energy Systems Annex 60 Final Report, 2017. URL: http://www.iea-annex60.org/downloads/iea-ebc-annex60-final-report.pdf.
[24] D. Müller, M. Lauster, A. Constantin, M. Fuchs, P. Remmen, Aixlib - an Open-Source Modelica Library Within the IEA-EBC Annex 60 Framework, in: Proc. CESBP Cent. Eur. Symp. Build. Phys. BauSIM 2016, Dresden, Germany, 2016, pp. 3–9.
[25] M. Wetter, W. Zuo, T. S. Nouidui, X. Pang, Modelica Buildings library, J. Build. Perform. Simul. 7 (2014) 253–270. doi:10.1080/19401493.2013.765506.
[26] F. Jorissen, G. Reynders, R. Baetens, D. Picard, D. Saelens, L. Helsen, Implementation and verification of the IDEAS building energy simulation library, J. Build. Perform. Simul. 11 (2018) 669–688. doi:10.1080/19401493.2018.1428361.
[27] C. Nytsch-Geusen, C. Banhardt, A. Inderfurth, K. Mucha, J. Möckel, J. Rädler, M. Thorade, C. R. Tugores, Buildingsystems - Eine modular hierarchische Modell-Bibliothek zur energetischen Gebäude und Anlagensimulation, in: CESBP Cent. Eur. Symp. Build. Phys. / BauSIM 2016, Dresden, Germany, 2016, pp. 473–480.
[28] J. Åkesson, K. E. Årzén, M. Gäfvert, T. Bergdahl, H. Tummescheit, Modeling and optimization with Optimica and JModelica.org-Languages and tools for solving large-scale dynamic optimization problems, Comput. Chem. Eng. 34 (2010) 1737–1749. doi:10.1016/j.compchemeng.2009.11.011.
[29] J. Drgoňa, L. Helsen, Different Problem Classes and Solution Techniques for Model Predictive Building Control, in: Proc. REHVA Annu. Meet. Conf. Low Carbon Technol. HVAC, Brussels, Belgium, 2018.
[30] J. Drgoňa, J. Arroyo, I. Cupeiro Figueroa, D. Blum, K. Arendt, D. Kim, E. P. Ollé, J. Oravec, M. Wetter, D. L. Vrabie, L. Helsen, All you need to know about model predictive control for buildings, Annu. Rev. Control 50 (2020) 190–232. doi:10.1016/j.arcontrol.2020.09.001.
[31] HSL. A collection of Fortran codes for large scale scientific computation., 2013. URL: http://www.hsl.rl.ac.uk/.
[32] A. Wächter, L. T. Biegler, On the implementation of an interior-point filter line-search algorithm for large-scale nonlinear programming, Math. Program. 106 (2006) 25–57. doi:10.1007/s10107-004-0559-y.
[33] M. Mork, A. Xhonneux, D. Müller, Nonlinear Distributed Model Predictive Control for multi-zone building energy systems, Energy Build. 264 (2022) 112066. doi:10.1016/j.enbuild.2022.112066.
[34] M. Mork, A. Xhonneux, D. Müller, Hierarchical Model Predictive Control for complex building energy systems, Bauphysik 42 (2020) 306–314. doi:10.1002/bapi.202000031.
[35] M. Mork, N. Materzok, A. Xhonneux, D. Müller, Nonlinear Hybrid Model Predictive Control for building energy systems, Energy Build. 270 (2022) 112298. doi:10.1016/j.enbuild.2022.112298.
[36] F. Redder, P. Althaus, L. Westphal, T. Storek, E. Ubachukwu, S. Johnen, M. Oden, A. Xhonneux, D. Müller, IoT Architecture for Monitoring and Control of Sector-coupled Energy Systems in a Real-life Laboratory: Conceptualization, Implementation and Evalution (Manuscript in Preparation) (2022).
[37] P. Althaus, F. Redder, E. Ubachukwu, M. Mork, A. Xhonneux, D. Müller, Enhancing Building Monitoring and Control for District Energy Systems: Technology Selection and Installation within the Living Lab Energy Campus, Appl. Sci. 12 (2022). doi:10.3390/app12073305.
[38] W. F. Holmgren, C. W. Hansen, M. A. Mikofski, pvlib python: a python package for modeling solar energy systems, J. Open Source Softw. 3 (2018) 884. doi:10.21105/joss.00884.
[39] S. Dervishi, A. Mahdavi, Computing diffuse fraction of global horizontal solar radiation: A model comparison, Sol. Energy 86 (2012) 1796–1802. URL: https://linkinghub.elsevier.com/retrieve/pii/S0038092X12001132. doi:10.1016/j.solener.2012.03.008.
[40] E. L. Maxwell, A quasi-physical model for converting hourly Global Horizontal to Direct Normal Insolation, SERI/TR-215-3087, Solar Energy Research Institute, 1987.
[41] D. Erbs, S. Klein, J. Duffie, Estimation of the diffuse radiation fraction for hourly, daily and monthly-average global radiation, Sol. Energy 28 (1982) 293–302. doi:10.1016/0038-092X(82)90302-4.
[42] D. T. Reindl, W. A. Beckman, J. A. Duffie, Diffuse fraction correlations, Sol. Energy 45 (1990) 1–7.
[43] J. Orgill, K. Hollands, Correlation equation for hourly diffuse radiation on a horizontal surface, Sol. Energy 19 (1977) 357–359. doi:10.1016/0038-092X(77)90006-8.
[44] R. R. Perez, P. Ineichen, E. L. Maxwell, R. D. Seals, A. Zelenka, Dynamic global-to-direct irradiance conversion models, ASHRAE Trans. 98 (1992) 354–369.
[45] F. Sun, G. Li, J. Wang, Unscented Kalman Filter Using Augmented State in the Presence of Additive Noise, in: 2009 IITA Int. Conf. Control. Autom. Syst. Eng. (case 2009), 3, IEEE, 2009, pp. 379–382. doi:10.1109/CASE.2009.51.
[46] E. Wan, R. Van Der Merwe, The unscented Kalman filter for nonlinear estimation, in: Proc. IEEE 2000 Adapt. Syst. Signal Process. Commun. Control Symp. (Cat. No.00EX373), IEEE, 2000, pp. 153–158. doi:10.1109/ASSPCC.2000.882463.
[47] DIN EN 12464-1. Light and lighting - Lighting of work places - Part 1: Indoor work places. German institute for standardization., 2011.